FLUX-SURFACE AVERAGED RADIAL TRANSPORT IN TOROIDAL PLASMAS WITH MAGNETIC ISLANDS

D. López-Bruna[1], B. Momo[2], I. Predebon[2], A. López-Fraguas[1], F. Auriemma[2] and Y. Suzuki[3,4]

[1]Laboratorio Nacional de Fusión – CIEMAT, Avda. Complutense 40, 28040 Madrid, Spain
[2]Consorzio RFX, corso Stati Uniti 4, 35127 Padova, Italy
[3]National Institute for Fusion Science, National Institutes of Natural Sciences, Toki, Gifu 509-5292, Japan
[4]SOKENDAI, The Graduate University for Advanced Studies, 322-6 Oroshi-cho, Toki 509-5292, Japan

Email contact main author: daniel.lopezbruna@ciemat.es

Abstract

In toroidal magnetic confinement fusion research, one-dimensional (1D) transport models rely on one radial coordinate that labels nested toroidal flux surfaces. The presence of magnetic islands in the magnetic geometry does not impede making 1D transport calculations if the island regions are excluded and then, if necessary, treated separately. In this work we show a simple way to modify the flux-surface coordinate and corresponding metric coefficients when an island region is excluded. Comparison with the metrics obtained from Poincaré plots are shown, as well as applications to two types of plasma: Heliac (TJ-II, CIEMAT, Spain), where the geometrical effects alone cannot explain the experimental results when islands move throughout minor radius; and Heliotron (LHD, NIFS, Japan), where we estimate the effect of possible heat losses in flux-gradient relations.

1. INTRODUCTION

In toroidal magnetic confinement fusion research, one-dimensional (1D) transport models rely on one radial coordinate that labels nested toroidal flux surfaces. Corresponding 1D transport codes are widespread tools to interpret and analyze experimental data, to check transport theories and, eventually, they can become fundamental pieces of real-time plasma control in a fusion reactor. However, geometrical issues might impede the use of 1D codes in the important cases where the topology of the assumed set of nested toroids is significantly broken, as it happens when magnetic island chains or chaotic layers develop. Not only should it be recalled that some topology breaking always happens at small enough spatial scales [1], but the size and location of island chains or chaotic layers can change depending on the evolution of plasma parameters, which, in turn, can be affected by the effect of topology breaking on transport. Doing transport in these cases would require, at least, properly updating the magnetic field configurations and corresponding metric coefficients: a complicated task. It is therefore desirable having a way to still perform traditional 1D transport analysis in these cases even if some simplification has to be assumed.

2. MODEL

For clarity, from now on we concentrate on the case of having one magnetic island chain with well-defined helicity. The presence of these islands does not preclude 1D transport calculations if the island regions are excluded. Of course, eliminating the island region implies loosing some plasma volume from the calculations, which will have to be treated separately if necessary. Let us start, then, with the modification of the flux-surface coordinate and the metric coefficients that affect "radial" transport when an island chain is taken away from the transport problem. We assume magnetic configurations with a well defined flux-surface coordinate $\rho_0 = \sqrt{\Phi_0/\Phi_{0a}}$ in the whole plasma domain, where $\Phi_0(\mathbf{x})$ represents the usual enclosed toroidal flux and Φ_{0a} is the value at any point of the last closed flux surface. A low order rational of the rotational transform ι is found at $\rho_{0s} = \sqrt{\Phi_{0s}/\Phi_{0a}}$. The opening of islands around ρ_{0s} deforms the flux surfaces *outside* the separatrix, but a set of nested toroids $\Phi(\mathbf{x})$ and corresponding $\bar{\rho}_0 = \sqrt{\Phi/\Phi_{0a}}$ can still be defined even if the meaning is no longer "enclosed toroidal flux" around the
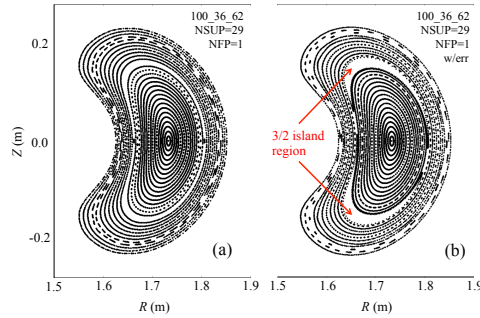
FIG. 1: *Poincaré plot at toroidal angle $\varphi = 0$ for a TJ-II vacuum configuration without (a) and with (b) error field to produce islands around the $\iota = 3/2$ magnetic resonance.*

resonant region. It is often the case that transport codes are based on magnetic configurations obtained from magnetic fields where some magnetic island chain is present, but still the configurations are described with a set of nested toroids. This can be taken as a common example of the coordinate $\bar{\rho}_0$ on which we apply the piecewise transformation due to eliminating the toroidal flux through the island-chain region, Φ_I. We define

$$\rho = \begin{cases} \sqrt{\frac{\Phi}{\Phi_{0a} - \Phi_I}}; & \Phi < \Phi_- \equiv \text{ toroidal flux enclosed by inside separatrix} \\ \sqrt{\frac{\Phi - \Phi_I}{\Phi_{0a} - \Phi_I}}; & \Phi > \Phi_+ \equiv \text{ toroidal flux enclosed by outside separatrix} \end{cases} \tag{1}$$

where we consider the separatrix as consisting of two surfaces: inside (facing the plasma center) and outside (facing plasma edge) separatrices connected at the X-point lines, which enclose respective fluxes Φ_- and Φ_+. Since $\Phi_I = \Phi_+ - \Phi_-$, it is a simple exercise [2] finding the corresponding transformation:

$$\rho = \begin{cases} \gamma \bar{\rho}_0; & \bar{\rho}_0 < \bar{\rho}_{0-} \\ \gamma \bar{\rho}_0 \sqrt{1 - \beta^2/\bar{\rho}_0^2}; & \bar{\rho}_0 > \bar{\rho}_{0+}, \end{cases} \tag{2}$$

where $\beta^2 \equiv \Phi_I/\Phi_{0a} < 1$ and $\gamma \equiv \sqrt{1/(1 - \beta^2)} \geq 1$. The definition Eq. 1 can be visualized as the consequence of eliminating an annulus of flux in the (ρ, θ) plane, where θ is a poloidal angle. For this reason, we shall refere to the model as "annular".

The transformation Eq. 2 implies discontinuities in the radial fluxes, which does not impede their numerical evaluation as we have checked by comparison with a code, based on the Multiple Domain Scheme, that calculates transport separately in the core, island and outer regions accounting for the evolution of the magnitudes at the separatrix [3]. Observe that, if discontinuities in the fluxes are allowed, the transport in the island region can be solved separately and taken into account as an additional term in the discontinuities of the fluxes. This might be important if thermodynamic gradients can evolve in the island region. Otherwise, as in steady state cases, only the particle and heat flux source/sink terms in the island region have to be considered in order to correctly compute balances.

The transformation of the flux surface averaged metric coefficients according to Ec. 2 can be compared with the results obtained directly from Poincaré plots. Flux-surface coordinates for TJ-II magnetic configurations are routinely obtained from a set of codes and libraries previously confronted with magnetic surface mapping experiments [4]. We have chosen a vacuum magnetic configuration that belongs to the operation set of the TJ-II Heliac. Its rotational transform is such that $\iota = 3/2$ around mid-plasma radius. Its Poincaré section at the toroidal angle $\varphi = 0$ is plotted in Fig. 1 (a). From this configuration we obtain the original coordinate $\bar{\rho}_0$ and the flux-surface averaged diagonal metric element $\langle g^{\bar{\rho}_0 \bar{\rho}_0} \rangle$, from which we obtain the new $\langle g^{\rho\rho} \rangle$ based on Ec. 2. Adding a small error field we obtain the Poincaré section shown in figure 1 (b). The existence of the low-order $\iota = 3/2$ in the unperturbed configuration promotes the onset of a vacuum $m = 2$ island chain for which we want to obtain directly the metric coefficients in the two regions at both sides of the separatrix. This has been done with a new code also based on fitting Poincaré maps at several toroidal cuts [5].

Figure 2 shows the comparison between the metric coefficients calculated numerically (dots) from the Poincaré sections and the results obtained analytically from the transformation 2 (continuous lines) with
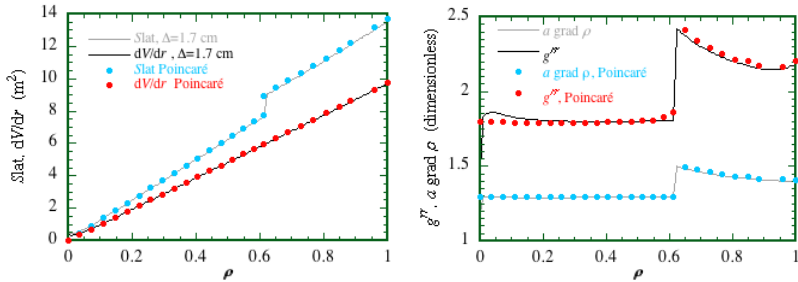
FIG. 2: *Volume radial derivative* dV/dr, $S_{\text{lat}} = \langle|\nabla r|\rangle dV/dr$ *(left)*, $\langle|\nabla r|\rangle$ *and* $\langle g^{rr}\rangle$ *(right) computed using the analitical annular model with island width* $\Delta = 1.7$ *cm (continous lines) and fits to Poincaré plots (dots) as in figure 1 (b). Here* $r \equiv a\rho$ *where* a *is the effective minor radius, e.g.* $dV/dr = (1/a)dV/d\rho$.

a value for β based on a cylindrical prescription for the island flux, $\beta^2 \propto \Delta$, where Δ is a measure of the average island width [2]. The good accordance is due to the fact that the main change is due to the loss of volume, not to the deformation of the flux surfaces near the resonant zone.

3. TRANSPORT EXAMPLES

Eq. 2 and the corresponding changes in the metric coefficients have been included in the ASTRA shell [6], with which we have worked application examples with two types of plasma: Heliac (TJ-II, CIEMAT, Spain); and Heliotron (LHD, NIFS, Japan).

3.1 Geometrical effect of magnetic islands on transport in TJ-II plasmas with evolving rotational transform

Here we present an example of predictive transport analysis in order to study how the opening of islands may affect the results due *only* to geometrical effects. The results are to be compared with well established results in TJ-II plasmas heated by EC-waves: low order rationals of ι leave a distinguishable trace in T_e-gradients when such "rationals" move through minor radius. This has been checked independently using Electron Cyclotron Emission (ECE) and Thomson Scattering diagnostics, and also different means of scanning the magnetic configuration (see a brief summary in[7]).
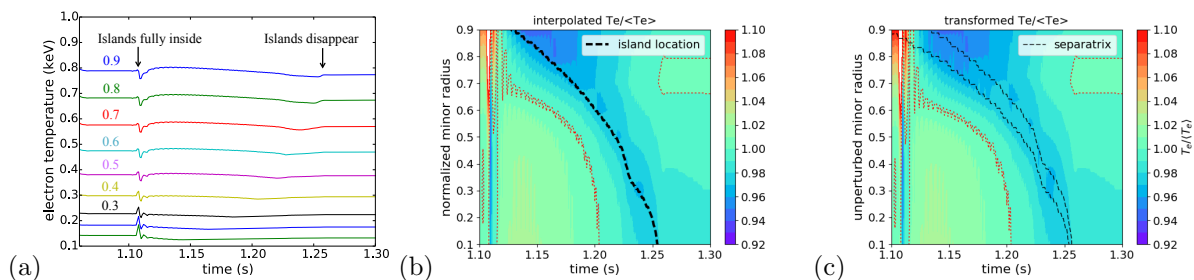

FIG. 3: (a) Time traces of $T_e(\rho)$ for equally spaced ρ values ranging from 0.1 to 0.9 in normalized minor radius during a simulated dynamic configuration scan; (b) evolution of the corresponding temperature profiles normalized to the time average, $T_e(\rho)/\bar{T}_e(\rho)$, as a function of the new coordinate. The black dashed line represents the path followed by the $\iota = 8/5$ rational through minor radius during the scan. Thin dotted lines indicate $T_e(\rho) = \bar{T}_e(\rho)$. (c) Evolution of $T_e(\bar{\rho}_0)/\bar{T}_e(\bar{\rho}_0)$, a function of the original coordinate. Values between the separatrix lines (thin black dashes) are not calculated.

In TJ-II experiments with variable magnetic configuration, the offset of the ι-profile is changed continuously during the discharge so that selected rationals are moved through minor radius [8]. We have set

a transport model that mimics steady state T_e-profiles of ECH TJ-II plasmas for the given electron heat source and density profiles. The electron heat transport is dominated by neoclassical loses and we impose the movement of the $\iota = 8/5$ rational from edge to core during the simulation. In order to make an island width that decreases with minor radius, we have set $\Delta = 1.5\rho$ cm, so the maximum effective width of 1.5 cm happens near the edge and decreases until collapsing at $\rho = 0$. Figure 3 (a) shows time traces of the simulated T_e at different radial positions in the transformed ρ coordinate. Initially, the islands are placed at $\rho = 0.975$ and there is just some loss of plasma volume but no discontinuity in the fluxes. At $t = 1.107$ s the islands are fully inside and the temperatures suffer a sharp change due to the sudden appearance of a discontinuous heat flux. During the time interval $1.107 < t < 1.257$ s the temperatures near the resonance tend to decrease; finally, when the rational $\iota = 8/5$ vanishes from the plasma ($t > 1.257$ s) the steady state is recovered and ρ is equivalent to the unperturbed original coordinate $\bar{\rho}_0$.

The evolution described above can be neatly visualized by following the evolution of the profile $T_e(\rho)/\bar{T}_e(\rho)$, where $\bar{T}_e$ is the mean value during the whole time interval, see figure 3 (b). We can appreciate that the change in the geometry implies lower temperatures around the rational, $T_e(\rho) < \bar{T}_e(\rho)$ (red dots indicate $T_e(\rho) = \bar{T}_e(\rho)$). For comparison, we have also plotted this normalized profile as a function of the original coordinate $\bar{\rho}_0$ in figure 3 (c), where the inside and outside parts of the separatrix are indicated with thin black dashes. Values between these lines are not calculated.

The results shown in Fig. 3 are *opposite* to what was found in the experiments [9]: local temperatures above the mean follow the rational. Namely, the present exercise with the island-modified geometry indicates that the change in electron temperatures found experimentally should be related with an *improvement* of confinement, at or by the magnetic resonance, not by geometrical effects.

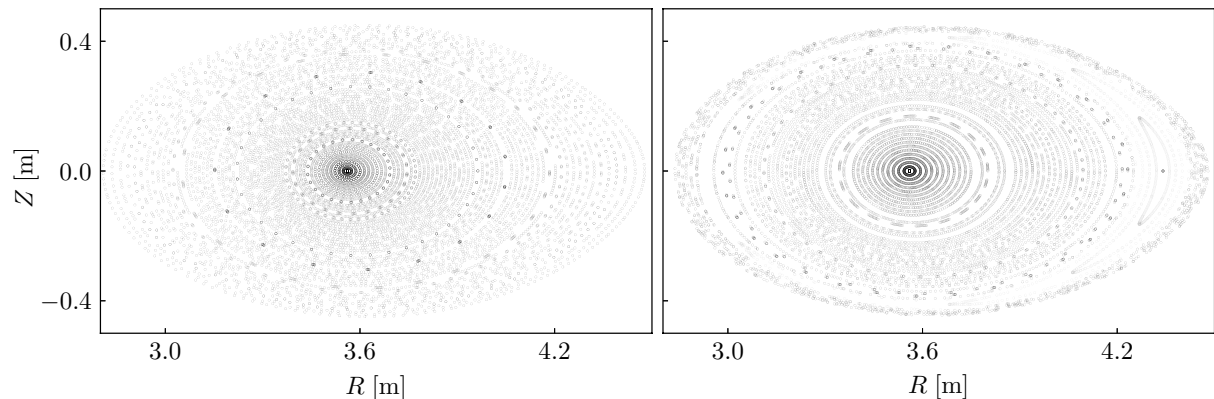## 3.2 Consequences of energy sink at the island regions in LHD magnetic configurations

FIG. 4: Poincaré plot of a low-β LHD magnetic configuration (major radius $R_{\mathrm{ax}} = 3.6$ m) without (left) and with externally driven 1/1 island (right).

This second example shows the use of the annular model to convert diagnostic coordinates and perform transport analyses without the need of re-calculating equilibria. Several experiments in the LHD make use of the driven 1/1 island, which opens near the plasma edge as can be seen in figure 4. Here we show the Poincaré plots for two configurations, the unperturbed one where we define the coordinate $\bar{\rho}_0$ (left) and the perturbed one that forces the opening of the near-edge island (right). As with TJ-II configurations, we have checked that the metric magnitudes obtained either by the transformation Eq. 2 or directly from sets of Poincaré plots of the perturbed configuration [5] are very similar [2]. In effect, this is obtained as long as a suited width ($\Delta = 7.6$ cm in this case) is chosen for the transformation. Note that the equatorial island width in figure 4 is about 12 cm. Similarly to the TJ-II configuration (figure 1), the value of Δ turns out quite representative of the actual average island width.

In order to do transport analysis outside the resonant region we use the metric profiles from the annular model. The starting, unperturbed configuration is obtained from VMEC giving rise to the normalized
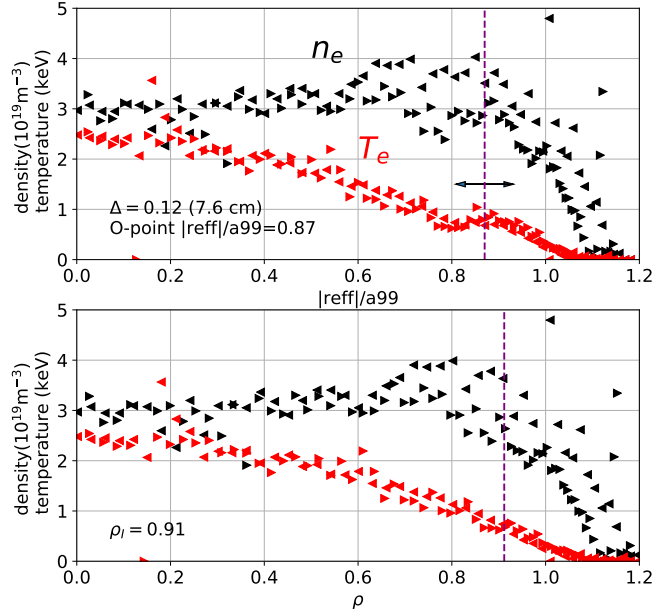
FIG. 5: *Thomson Scattering electron density (black) and temperature (red) profiles for LHD discharge #140534 at t = 4 s. Top: original data from negative (◄) and positive (►) Thomson radius in the normalized coordinate $|r_{\mathrm{eff}}/a_{99}|$. A vertical dashed line indicates the center of the $\iota = 1$ resonance and a double-arrow its width Δ. Error bars are not drawn for clarity. Bottom: The same data after eliminating the resonant region through the transformation Eq. 2. The location of the separatrix (vertical dashed line) has a new effective radius.*

effective coordinate $\bar{\rho}_0 \equiv r_{\mathrm{eff}}/a_{99}$, to which several diagnostics are referred. Here we transform the input kinetic profiles from Thomson Scattering data of LHD discharge No. 140534 (figure 5 top) and take away the data that fall in the resonant region spanned by the horizontal arrow. The remaining data and coordinate values are mapped onto the radial coordinate ρ, which eliminates the island part of the profiles thus rendering them continuous and monotonic, see figure 5 (bottom). We can now perform transport studies on these profiles. In particular, LHD discharge #140534 around $t = 4$ s corresponds to a base plasma sustained by NBI heating with superimposed modulated ECH (MECH) at 20 Hz with a square wave-form. We have set a diffusive transport model with neoclassical χ_e^{NC} following the formulation used in [10], and a simple function $\chi_e^a = C\rho^8$ for the edge zone, where C is a constant. Heat sources have not been calculated but taken as Gaussian profiles with different normalizations so as to obtain the respective heating powers of the selected discharge at $t = 4$ s (net NBI power $Q_{\mathrm{NBI}} = 15.8$ MW, ECH amplitude $Q_{\mathrm{ECH}} = 1.4$ MW). The widths and centering of the Gaussians have been adjusted so the source profiles are similar to those shown in [11]. Efficiency factors in the heating have been set so as to mimic the evolution of the experimental temperature at $R = 3.861$ m, corresponding to $\rho(\bar{\rho}_0 = 0.27) = 0.3$ around $t = 4$ s, as shown in figure 6.

Heat pulse propagation experiments with localized central heating where the delay time is not monotonic with radius (e.g. [11]) are naturally reproduced with this model (outside the island region) because of the unique coordinate for the separatrix. If non-trivial transport calculations are necessary inside the island, they should be separately done as in [3]. A clear advantage of the annular model is that we can study the possible effect of other islands in MECH experiments without the need of re-calculating the metrics from Poincaré plots. Once the T_e response to MECH is fairly reproduced (figure 6), we investigate a possible effect of opening islands around mid-radius due to the resonance $\iota = 1/2$. Taking Ref. [12] as example, we use the annular model to change the island position: without re-doing the Poincaré sections we set an effective island width of 5 cm at the location of $\iota = 1/2$, around mid-radius. As in [12], we use different amplitudes for the MECH power, from 1 to 3 MW, with narrow Gaussian centered around $\rho = 0.1$. Then we set a diagnostic for the "experimental" heat flux normalized by the electron density at ρ,

$$\frac{q_e^{\mathrm{exp}}}{n_e}(\rho) = -\frac{1}{n_e S} \int_0^\rho \mathrm{d}\rho' V' \left[\frac{3}{2} n_e \partial_t T_e - P_{\mathrm{ECH}} - P_{\mathrm{NBI}} \right]. \tag{3}$$
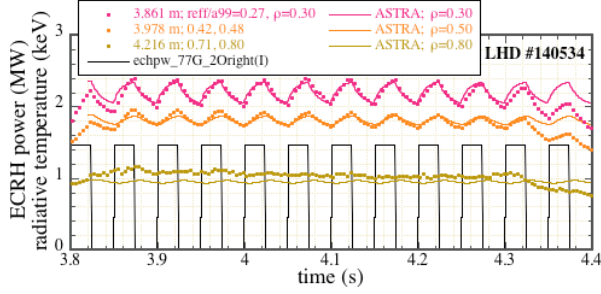
FIG. 6: *Time traces of the electron temperature around t = 4 s for LHD discharge #140534 (dots) and calculated values using ASTRA (lines). The labels show the corresponding laboratory coordinate R, the original $\rho_0 = r_{\mathrm{eff}}/a_{99}$ and the transformed ρ according to figure 5. The modulated ECH power is shown with black lines.*
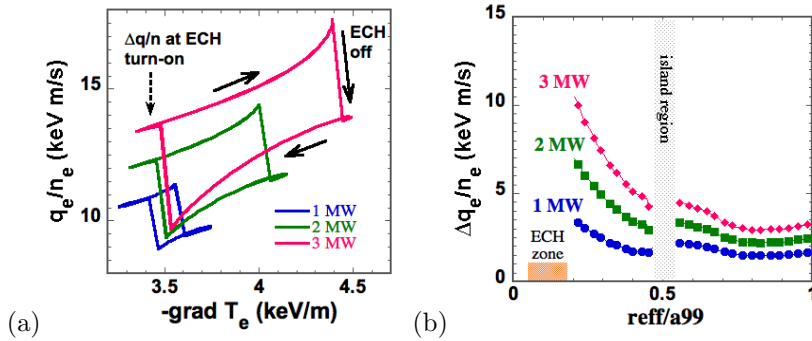

FIG. 7: *(a) Flux-gradient relation at $\rho = 0.6$ according to Eq. 3 for a transport simulation with heat source Eq. 4 at three different nominal ECH powers. (b) Corresponding profiles, in terms of the radial coordinate $\bar{\rho}_0 \equiv r_{\mathrm{eff}}/a$, of the jump at the time of ECH turn-on.*

Here all magnitudes, electron density n_e, temperature T_e, power densitites, area S of the flux surface and $V' = \mathrm{d}V/\mathrm{d}\rho$, are profiles. P_{ECH} is a *nominal* ECH power under the assumption of 100% absorption.

Inspired by TJ-II results on the effects of ECH on the electrons, in the present exercise we hypothesize that the electron heat balance includes two heat sinks: one is due to direct ripple losses at the injection region, which basically is a correction to the nominal deposited power $\eta_{\mathrm{rl}}P_{\mathrm{ECH}}$ with $\eta_{\mathrm{rl}} < 1$ [13]; another one corresponds to fast electrons that can accumulate with very long confinement time in the resonant zone [14], in our case related with $\iota = 1/2$ around $\rho_s \approx 0.5$. In terms of transport, the latter provide a sink around the resonant region where the islands open. Even if these electrons are very few comparatively, their energies can be very high, say tens of keV, and thus represent a non-negligible power density sink P_{isl} for the plasma outside the islands zone. In order to account for these effects, in the transport calculations we set a source/sink term

$$P_e(\rho) = \eta_{\mathrm{rl}}P_{\mathrm{ECH}}(\rho) - P_{\mathrm{isl}}(\rho) \tag{4}$$

where $P_{\mathrm{isl}}(\rho)$ is a peaked function centered at ρ_s. This term, as all ECH power terms, is modulated as in figure 6.

Figure 7 (a) represents the flux-gradient relationship obtained using the diagnostic Eq. 3 for a simulation of the plasma with P_e as in Eq. 4 using the same model for transport fluxes used in figure 6, i.e., a mostly neoclassical description of the electron heat transport except near the edge. The three closed curves correspond to the indicated simulated *nominal* ECH powers, $\int \mathrm{d}V P_{\mathrm{ECH}}$. Arrows indicate the evolution of the curve for the 3 MW case, which is qualitatively the same as the other curves. Each time the MECH is turned on there is a jump $\Delta q^{\mathrm{exp}}/n_e$ due to the unbalance between the time derivative term and the nominal power P_{ECH} in Eq. 3. Such jump, as well as the covered range of T_e-gradients, increases with nominal power. The magnitude of the jump varies at each radial location giving rise to the profiles

shown in Figure 7 (b) for the same cases in terms of the radial coordinate $\bar{\rho}_0 \equiv r_{\text{eff}}/a$ obtained with the inverse of transformation 2. Outside the MECH zone, and considering a modulation period on the order of the energy confinement time, the jump is given by the excess power between the nominal P_{ECH} and P_e in Eq. 4,

$$\Delta \frac{q_e^{\text{exp}}}{n_e} \approx \int_0^\rho \mathrm{d}\rho V'[P_{\text{ECH}} - P_e] = \int_0^\rho \mathrm{d}\rho V'[(1 - \eta_{\text{rl}})P_{\text{ECH}} + P_{\text{isl}}].$$

The calculations in the appropriate geometry allow for a quantitative estimate of these effects. In the case of figure 7 we have, for all cases, $\eta_{\text{rl}} = 0.7$ and $\int \mathrm{d}V P_{\text{isl}} = 0.3$ MW. The latter is responsible for the increment in $\Delta q^{\text{exp}}/n_e$ when crossing the island region in figure 7 (b).

The present exercise has been developed as an application example of the transformations due to the annular model. Consequently, the transport analysis yielding figure 7 cannot be considered as representative of any particular LHD discharges. However, we see how the consideration of island regions may provide a contribution to experimental results as those shown in [12]. The consideration of the appropriate metric and estimates of the power density profiles, Eq. 4, should help to better quantify the effects attributed to turbulence in the experimental hysteresis loops.

4. SUMMARY

1D transport analyses in toroidal plasmas where island chains are present can be done after eliminating the latter from the transport domain. We have developed a coordinate change that reduces the problem to the region outside the islands, where a flux surface radial coordinate can be defined in the usual way, at the expense of having discontinuous radial fluxes. The resulting metric magnitudes (e.g. radial derivative of the volume, $\mathrm{d}V/\mathrm{d}\rho$, and flux-surface averaged diagonal metric coefficient, $\langle g^{\rho\rho}\rangle$) agree well with the values obtained directly from Poincaré plots if a proper average island width is provided. By comparison with a transport code based on a Multiple Domain Scheme, and therefore free from discontinuities, we have also checked that a 1D transport code (ASTRA in our case) can handle the discontinuous fluxes satisfactorily. Finally, we have worked application examples considering two types of helical device: the TJ-II Heliac, where we find that the geometrical effects alone cannot explain the experimental observations when the islands move throughout minor radius in ECH plasmas; and the LHD Heliotron, where we propose an exercise to quantify the heat losses that would give rise to discontinuous flux-gradient relations in plasmas with modulated ECH in presence of an island region acting as a heat sink.

ACKNOWLEDGEMENTS

REFERENCES

[1] GRAD, H., Phys. Fluids **10** (1967) 137.

[2] LÓPEZ-BRUNA, D., et al., Nucl. Fusion **58** (2018) 106031.

[3] AURIEMMA, F., et al., Nucl. Fusion **58** (2018) 096037.

[4] LÓPEZ-FRAGUAS, A., et al., "Magnetic surface mapping in TJ-II heliac", Proc. 13th Intl. Stell. Workshop (Canberra, Australia) PI.6, 2002.

[5] PREDEBON, I., MOMO, B., SUZUKI, Y., AURIEMMA, F., Plasma Phys. Control. Fusion **60** (2018) 045003.

[6] PEREVERZEV, G. V., YUSHMANOV, P. N., "ASTRA Automated System for TRansport Analysis", Tech. Rep. IPP 5/98, Max Plank Institut für Plasmaphysik, Garching, February 2002.

[7] LÓPEZ-BRUNA, D., et al., VARGAS, V. I., ROMERO, J. A., J. Phys.: Conf. Series, **591** (2015) 012013.

[8] LÓPEZ-BRUNA, D., et al., Nucl. Fusion **49** (2009) 085016.

[9] LÓPEZ-BRUNA, D., et al., Plasma Phys. Control. Fusion **53** (2011) 124022.

[10] GARCIA, J., DIES, J., CASTEJON, F., YAMAZAKI, K., Phys. Plasmas **14** (2007) 102511.

[11] IDA, K., et al., New J. Phys. **15** (2013) 013061.

[12] INAGAKI, S., et al., Nucl. Fusion **53** (2013) 113006.

[13] OCHANDO, M. A., MEDINA, F., the TJ-II TEAM, Plasma Phys. Control. Fusion **45** (2003) 221.

[14] OCHANDO, M. A., et al., "Confinement of fast electrons at rational surfaces in the TJ-II stellarator", in Proc. 12th IAEA Int. Stellarator Workshop, (Madison (WI) USA), 1999.